Mon. Not. R. Astron. Soc. **260,** 705–716 (1993)

Power spectrum of the matter distribution in the Universe on large scales

Jaan Einasto,[1,2] Mirt Gramann,[1,2] Enn Saar[1] and Erik Tago[1]

[1] *Tartu Astrophysical Observatory, EE-2444 Tõravere, Estonia*
[2] *European Southern Observatory, D-8046 Garching, Germany*

Accepted 1992 June 25. Received 1992 June 17; in original form 1992 March 31

ABSTRACT

The power spectrum of the distribution of clusters of galaxies in the northern and southern galactic hemispheres has been evaluated. Corrections have been applied for the smoothing effect, and for the Poisson noise. The effects of incompleteness of data and observational errors have been investigated. The cluster spectrum has been transformed to galaxy and matter power spectra. Data suggest that the power spectrum has an index $-2 \leq n \leq -1$ on intermediate scales; on very large scales the spectrum is consistent with the Harrison–Zeldovich index $n = 1$. The transition from the Harrison–Zeldovich index to a lower index occurs at the scale $\lambda_t \approx 150 \pm 50\ h^{-1}$ Mpc. Direct comparison of the samples used and power-spectrum analysis suggest that our samples approach the size of fair samples of the Universe.

Key words: galaxies: clustering – large-scale structure of Universe.

1 INTRODUCTION

The statistical properties of the density field of the Universe can be described by the correlation function, or by its Fourier transform, the power spectrum of density fluctuations. Both approaches have their advantages and disadvantages, as discussed by Peebles (1973, 1980) and more recently by Baumgart & Fry (1991, hereafter BF) and by Peacock & Nicholson (1991, hereafter PN). In studying the evolution of the structure, the input function is the power spectrum. Usually it is given from theoretical considerations based on hypotheses on the nature of dark matter. On large scales, the density fluctuations continue to grow in the linear regime and the spectrum retains its original shape.

BF, PN, Peacock (1991, hereafter P91) and Gramann & Einasto (1992, hereafter GE) analysed the power spectrum for various galaxy samples over the scale interval ≈ 1 to $\approx 200\ h^{-1}$ Mpc (here and below, distances correspond to the Hubble constant $H_0 = 100\ h$ km s^{-1} Mpc^{-1}). In a rather broad scale interval, the spectrum can be approximated as a power law with an index $-1 \geq n \geq -2$. On the largest scales, PN and P91 find a departure from the power law which can be considered as a transition to a different spectral index. From theoretical considerations, it was assumed that on the largest scales the spectrum has a form predicted by Harrison and Zeldovich with index $n = 1$. Recent observations of fluctuations of the cosmic microwave background (CMB) radiation are consistent with this hypothesis (Smoot et al. 1992).

The presence and location of the transition in the power spectrum have important consequences for the theory of structure formation. It is evident that the determination of the power spectrum at scales larger than those previously considered is an attractive challenge. On scales of interest, clusters of galaxies are suitable objects with which to investigate the power spectrum.

The goal of the present paper is to evaluate the power spectrum from the distribution of clusters of galaxies. To determine the power spectrum from observations, we have to consider a number of technical problems: incompleteness of observational data, Poisson noise, the deviation of the cluster spectrum from the spectrum for the total matter, etc. We shall discuss these problems in detail in the next sections. In Section 2 we describe the data used and derive the power spectrum for cluster samples. In Section 3 we analyse the errors of the power spectrum. In Section 4 we derive the correlation function of cluster samples and compare our results with models. The paper ends with a discussion and short summary of principal results.

A short note on terminology is useful. The global spectrum, i.e. the spectrum of matter for a large representative or fair sample of the Universe, is of interest for theoretical purposes. Presently, we do not know the size of the observational sample needed to find the global spectrum. What we

obtain from observations are only estimates of the power spectrum. The same is true for the correlation function – from observations, we obtain its estimates. As is the practice with the correlation function, we also use the term 'power spectrum' for its observational estimates.

2 POWER SPECTRA FOR CLUSTER SAMPLES

2.1 Definitions

A fluctuating density field,

$$\delta(\boldsymbol{x}) \equiv \frac{\varrho(\boldsymbol{x}) - \overline{\varrho}}{\overline{\varrho}}, \tag{1}$$

can be described in terms of its Fourier components

$$\delta_k = \frac{1}{V}\int_V \delta(\boldsymbol{x}) \exp(i\boldsymbol{kx})\, \mathrm{d}^3 x, \tag{2}$$

where k denotes the comoving wavenumber ($k = 2\pi/\lambda$). Here $\varrho(\boldsymbol{x})$ is the density and $\overline{\varrho}$ is the mean density in the given volume. The power spectrum is defined as the square of the Fourier transform of the density contrast,

$$P(k) \equiv \left(\frac{L}{2\pi}\right)^3 \langle |\delta_k|^2 \rangle, \tag{3}$$

where L is the size of the cubic box of volume V under study.

An alternative method for describing the density field is to use the autocorrelation function of the density contrast (for simplicity we shall use the conventional term 'correlation function'),

$$\xi(r) \equiv \langle \delta(\boldsymbol{x})\, \delta(\boldsymbol{x}+\boldsymbol{r}) \rangle. \tag{4}$$

The power spectrum $P(k)$ and the correlation function $\xi(r)$ are directly related, forming a Fourier transform pair

$$\xi(r) = 4\pi \int_0^\infty P(k) \frac{\sin(kr)}{kr} k^2\, \mathrm{d}k, \tag{5}$$

$$P(k) = \frac{1}{2\pi^2} \int_0^\infty \xi(r) \frac{\sin(kr)}{kr} r^2\, \mathrm{d}r. \tag{6}$$

The spectrum P can be expressed as a function of either k or λ. Instead of P, one can also use a dimensionless variable Δ^2 [the contribution to the relative density per unit range of $\ln k$ (see PN)], where

$$\Delta^2 = 4\pi k^3 P(k) = 4\pi k^3 \left(\frac{L}{2\pi}\right)^3 \langle |\delta_k|^2 \rangle. \tag{7}$$

The shapes of functions Δ^2 and P are different – the dimensionless power spectrum Δ^2 has no maximum on large scales, but there is a change in the slope. In most cases, we shall use the function P and the wavelength λ as the argument. In Fig. 3 (see later), we use the wavenumber k as the argument.

2.2 Data on cluster samples

Our basic cluster sample was compiled by Tago & Einasto (1992) using all available redshift determinations for clusters of the new Abell, Corwin & Olowin (1989, hereafter ACO) catalogue. We have used the digitized version of the catalogue supplied by Olowin, since the printed version has errors in it. All available redshift sources were used, and the compilation was updated in 1992 January.

The version of the catalogue we used has the same columns as the original version of ACO with one addition: Tago & Einasto (1992) have calculated from photometric data an estimated redshift, z_{est}. When the magnitudes $m1$, $m3$ and $m10$ were available, the redshift estimate was found, as suggested by ACO, using all three magnitudes. When only $m10$ was available, the Leir & van den Bergh (1977) and Postman et al. (1985) prescripts were used. In the overlapping area of the northern and southern surveys, the new southern data were preferred. Some clusters enter the catalogue twice, in which case only one entry was used. The final catalogue contains 4072 clusters. For all clusters, the equatorial, galactic and supergalactic coordinates were calculated and, by adding redshift information, also the rectangular galactic coordinates. We prefer galactic coordinates, since in this case it is easier to specify unobserved regions near the galactic plane. Measured redshifts were used if they were available, unless it seemed probable that a foreground galaxy had been observed [these clusters are marked in ACO and Postman et al. (1985)]; in this case, the photometric distance was used. The total number of clusters with measured and accepted redshifts in the catalogue is 1065, and most measured redshifts belong to nearby clusters, $z \leq 0.1$.

From this catalogue, several cubic subsamples in certain galactic rectangular coordinate limits were chosen. In Table 1, we give the name of the subsample, the centre coordinates X_0, Y_0, Z_0, the sample size L, the number of clusters N_{cl}, the number of clusters with estimated redshifts N_{est}, and the correlation length r_0 of the sample. Distances correspond to the Hubble constant $H_0 = 100\ h\,\mathrm{km\,s^{-1}\,Mpc^{-1}}$.

To obtain unbiased estimates of the power spectra, we must take into account the fraction of space where clusters were actually observed. It is well known that at low galactic latitudes the strong galactic obscuration makes the observation of clusters impossible. The lower limit of the galactic latitude, b_0, and the fraction of space covered by observations, F_{obs}, is given in Table 1. In order to minimize the influence of galactic absorption, we used subsamples ACO2.5ND, ACO2ND, ACO2.5SD and ACO2SD, with one diagonal of the cube directed towards a galactic pole. In these samples, clusters located at low galactic latitudes are automatically excluded. We shall call these samples 'diagonal', and samples with boundaries parallel to the galactic plane, 'standard'.

For standard samples, we have used two sample sizes, $200\ h^{-1}$ and $300\ h^{-1}$ Mpc, and for diagonal samples, $200\ h^{-1}$ and $250\ h^{-1}$ Mpc. Smaller samples lie completely within the boundaries of larger samples and are used only to check the reliability of the statistical properties of samples.

In most previous studies, only clusters of richness class ≥ 1 have been included in samples for statistical studies, since clusters of richness class 0 may be affected by projection effects. We have included clusters of all richness classes. The motivation for this is the following. First, West & van den Bergh (1991) have studied the distribution of clusters of all richness classes containing cD galaxies or having

Table 1. Data on cluster samples.

Name	L	X_0	Y_0	Z_0	N_{cl}	N_{est}	b_0	F_{obs}	r_0
ACO2ND	200	0	0	173	95	4	45°	1.0000	24.5
ACO2SD	200	0	0	-173	142	37	45°	1.0000	25.7
ACO2.5ND	250	0	0	217	183	46	45°	1.0000	22.6
ACO2.5SD	250	0	0	-217	253	111	45°	1.0000	20.3
ACO2N	200	0	0	150	141	1	25°	0.9967	21.7
ACO2S	200	0	0	-150	153	31	25°	0.9967	14.2
ACO3N	300	0	0	200	351	104	25°	0.9657	23.5
ACO3S	300	0	0	-200	427	175	25°	0.9657	19.3

Bautz–Morgan types I and I–II. Both morphological types define clusters with high central densities which are without any doubt real clusters. A large fraction of these clusters belongs to richness class 0. Secondly, our own experience of the study of the Perseus–Pisces and Coma superclusters (Einasto, Jõeveer & Saar 1979; Tago, Einasto & Saar 1984) has shown that poor clusters as well as dense groups are very good tracers of the large-scale structure.

To obtain a visual impression of the distribution of clusters in our basic samples ACO3N and ACO3S, we plot in Figs 1 and 2 the distribution of clusters in four consecutive sheets, the respective Z-coordinate intervals being indicated in the figures.

A comparison of the figures shows that in the northern sample ACO3N the distribution is more clumpy. We see a number of prominent superclusters, such as the Shapley and

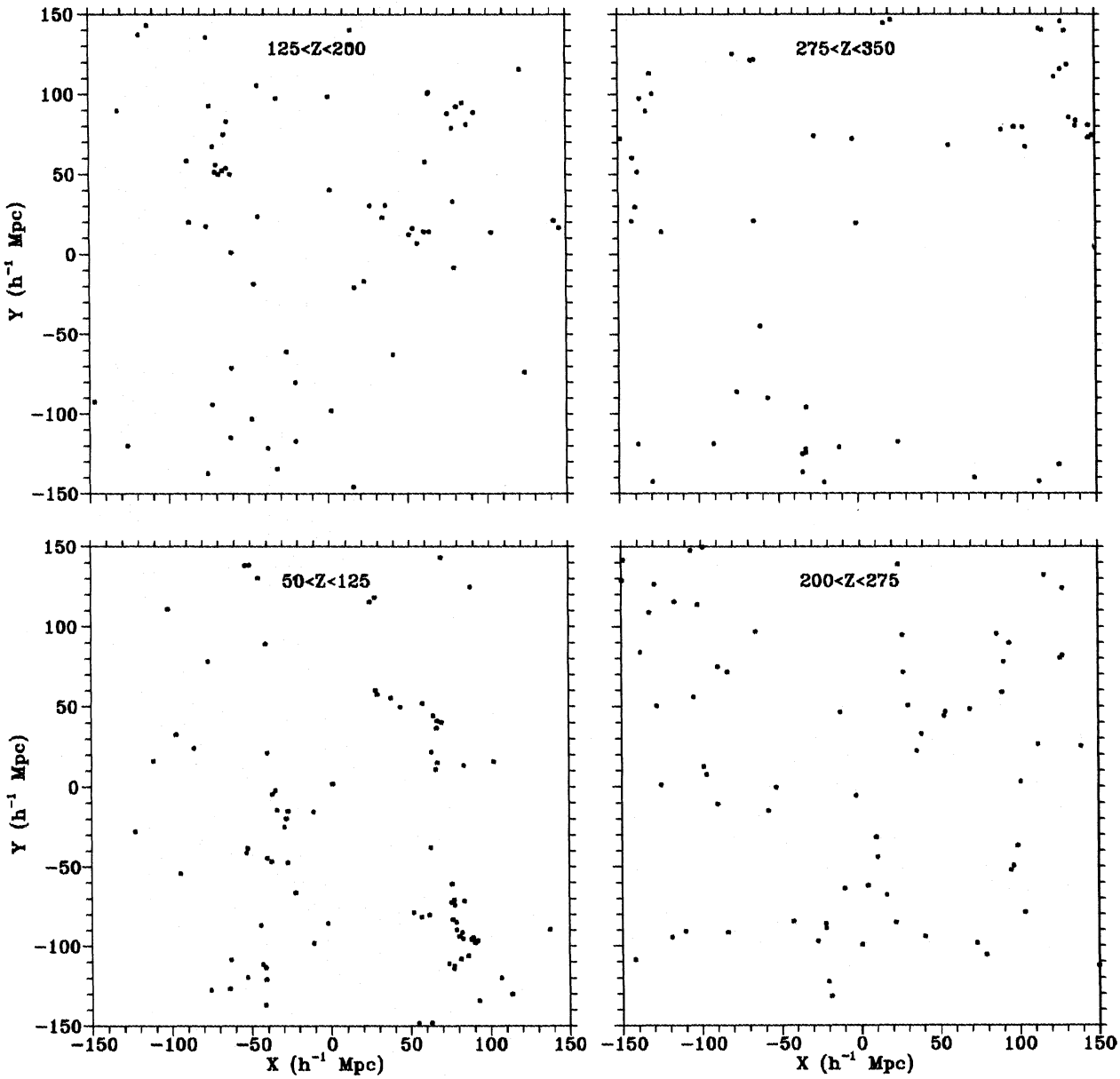

Figure 1. The distribution of clusters of the sample ACO3N in rectangular galactic coordinates in four sheets; respective Z-coordinate intervals are indicated.

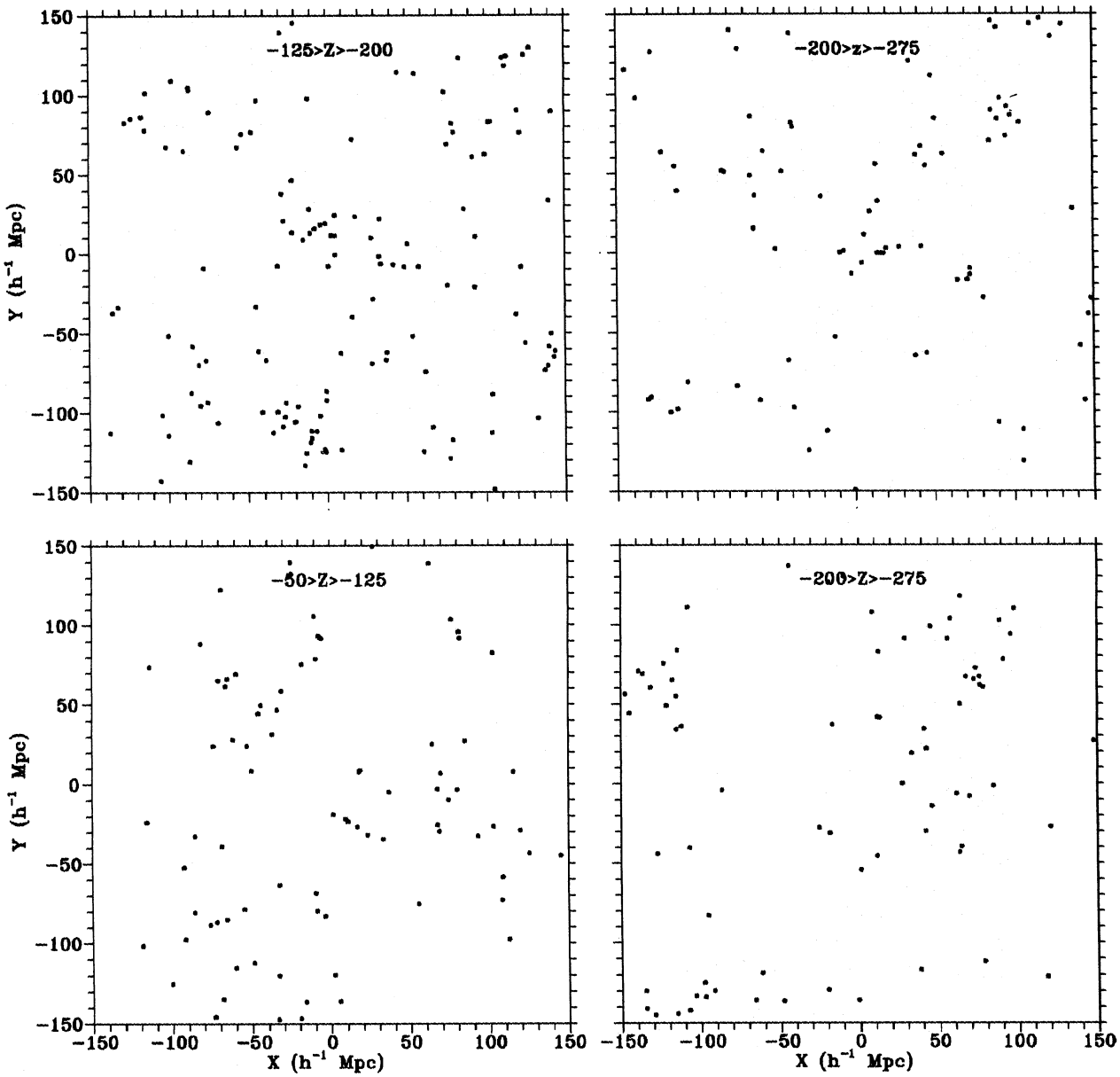

Figure 2. The distribution of clusters of the sample ACO3S in four sheets.

Hercules superclusters in the lower left panel (the concentration at $X \approx 80$, $Y \approx -100$, and $X \approx 70$, $Y \approx 40$, respectively). The distribution of clusters in the southern hemisphere is smoother. Here, there are no rich superclusters such as those seen in the northern hemisphere, and voids are not as empty as the voids in the northern sample. This is due in part to a much larger fraction of clusters with larger errors attached to their estimated redshifts.

For various checks, we have used two- and three-dimensional numerical simulations. These simulations have been described in detail by Gramann (1988, 1992); see also Section 4.3.

2.3 Determination of power spectra

We used two methods to calculate the power spectrum for cluster samples. First, the spectrum was determined from the smoothed density field by its Fourier transform; secondly, the Fourier transform was calculated using discrete positions of particles. The mathematical details and corrections applied are different in these cases, thus the application of independent methods allows us to check the validity of results.

The smoothed distribution of particles was used by GE in their study of the power spectrum of galaxies. In this case, the first step is the calculation of a smooth density field using the standard cloud-in-cell (CIC) procedure. The smoothing length is taken equal to the grid size, l, and is related to sample box size L as $L/l = 2^q$. For cluster samples and three-dimensional model samples, we used three different grid sizes corresponding to $q = 4$, 5 and 6; for two-dimensional samples, grid parameters $q = 4, 5, \ldots, 9$ were used. To find Fourier components of the density field, the fast-Fourier algorithm was applied (Hockney 1970). Periodic boundary conditions were adopted.

In the second method, we calculated the Fourier coefficients directly from the positions of individual galaxies. This is a straightforward procedure but has its price – for non-regularly spaced points we cannot use the fast-Fourier algorithm, and the conventional Fourier transform takes much more computation time than the fast algorithm. The discrete case is therefore applicable only for small samples, i.e. observed samples. For model samples, where the number of particles reaches hundreds of thousands, only the smooth density method can be used.

In both cases, for each value of k the value of the spectrum, P, was calculated by integrating the field δ_k^2 in a spherical (circular) layer of radii $[k-0.5,\ k+0.5]$. We were able to determine in a given volume up to 32 spectral modes on scales from L to $L/32$.

Uncorrected power spectra for cluster samples are shown in Fig. 3. Spectra were calculated for the resolution parameter $q=5$.

Now we have to consider the corrections to be applied to observed spectra. There are six possible sources of systematic errors in observed spectra: a smoothing effect (for spectra calculated from a smooth density field), the Poisson noise, the periodic boundary assumption made in calculating the Fourier transform, the incompleteness of observational data, and differences in the amplitudes and shapes of the power spectra of clusters and galaxies. We shall apply corrections for only part of these errors; in other cases, we estimate the range of possible errors.

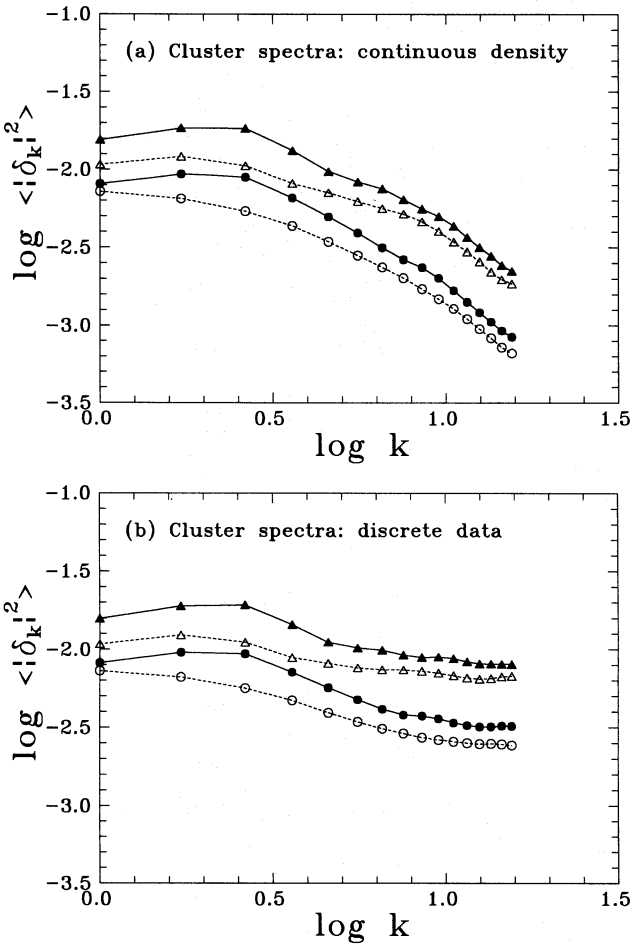

Figure 3. Uncorrected power spectra for samples ACO2N, ACO2S, ACO3N and ACO3S, calculated (a) with the continuous density method, and (b) from discrete distribution of particles. Circles denote 300-Mpc samples, triangles 200-Mpc ones; filled symbols correspond to northern, open symbols to southern samples.

2.4 Correction for grid smoothing

In calculating the power spectrum from a smooth density field, high-frequency spectral modes are suppressed due to smoothing. This introduces an error, which is easily seen in the left panel of Fig. 3 – the high-frequency end of the spectrum deviates downwards.

This smoothing effect is due to the convolution of the real density field in the CIC procedure, and the way to correct for it is well known – the spectra obtained have to be divided by the spectrum of the convolution function. This correction factor is evaluated in the Appendix.

2.5 Correction for the Poisson noise

After correction for the grid smoothing effect, all spectra of cluster samples are horizontal at large wavenumbers, $k>10$. This is due to the Poisson noise, which masks the actual spectrum at high frequencies. At lower frequencies, the cluster spectrum dominates but is influenced by the Poisson noise.

To correct for this effect, a constant term is subtracted from the observed spectrum. For spectra expressed in dimensionless units $\langle|\delta_k|^2\rangle$, this correction is equal to $1/N_{\rm cl}$, where $N_{\rm cl}$ is the number of objects in the catalogue (see Peebles 1980; PN).

Spectra obtained from the continuous density field and from discrete data using the corrections discussed above almost coincide. This demonstrates that our procedures to correct for data smoothing and for Poisson noise work satisfactorily.

2.6 Correction for sample boundaries

To calculate the correction for the sample boundaries, we shall use the method outlined by PN. The Fourier transform of the selection function was subtracted from the spectrum, and the whole spectrum was divided by the 'filling' factor $F_{\rm obs}=V_{\rm obs}/V$. Boundary selection removes only some of the edges of the computational volume, and the observed space forms a contiguous volume which fills a large fraction of the cube under study. Our calculations have shown that, if the fraction of the observed space is small ($F_{\rm obs}<0.5$), the spectrum at low wavenumbers (large scales) is dominated by the boundary effect and the determination of the actual spectrum of clusters is subject to large uncertainties. For this reason, we have chosen sample boundaries which minimize the correction. In our basic samples, the correction does not exceed 10 per cent of the observed value of the spectrum at the largest wavelengths; on smaller scales, the effect is negligible. In diagonal samples this effect is eliminated completely.

2.7 Mean cluster spectrum

The comparison of corrected cluster spectra of samples ACO3N and ACO3S (Fig. 4a) shows that the southern

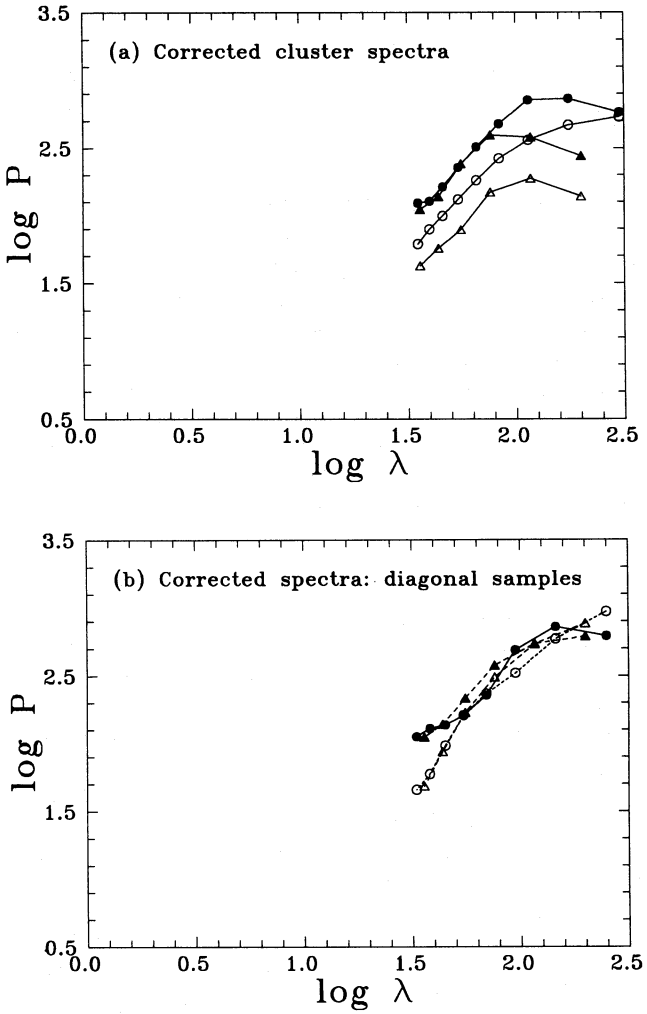

Figure 4. (a) Corrected spectra of standard cluster samples. Samples are designed as in Fig. 3. Here we use the function P as the power spectrum, found from equation (3). (b) Corrected spectra of diagonal samples. 250 h^{-1} Mpc samples are denoted by circles, 200 h^{-1} Mpc samples by triangles; for northern samples we use filled, for southern samples open symbols.

hemisphere samples, after all corrections, have spectra of lower amplitudes than the northern samples. On the other hand, the northern and southern diagonal samples ACO2.5N and ACO2.5S agree rather well (see Fig. 4b). In diagonal samples, no correction for incompleteness has been applied. The spectrum for the sample ACO3N is rather similar to the mean spectrum of samples ACO2.5N and ACO2.5S. Due to the large deviation of the spectrum ACO3S we shall not use it in the following analysis, and the overall mean is based on samples ACO3N, ACO2.5N and ACO2.5S. Smaller samples of 200-Mpc cube size serve only for comparison since their boundaries lie completely within the boundaries of large samples.

2.8 Reduction of cluster spectra to galaxy and matter spectra

Our goal is to reduce the cluster spectra to the spectrum of the matter. This can be accomplished in two steps, the first reducing the cluster spectrum to the galaxy spectrum, and the second calculating from the galaxy spectrum the spectrum for the whole matter.

On the basis of model calculations, Gramann & Einasto (1991) concluded that the power spectrum of the total matter, P_m, practically coincides with the spectrum for galaxies, P_g; the only correction to be applied is that which takes into account the fraction of matter associated with galaxies, F_g. We shall discuss this problem in more detail in Section 4.3. To calculate the power spectrum, we average over the square of the Fourier components of the density contrast, so, to normalize the galaxy spectrum for total matter, we must multiply it by the square of the fraction of matter associated with galaxies,

$$P_m = F_g^2 P_g. \tag{8}$$

We applied this formula to find the matter density spectrum. The fraction of matter in galaxies was taken as $F_g = 0.65$, following Einasto & Gramann (1991). The matter spectrum can be expressed analytically by the formula (12) (see below) with parameters $A = 98$, $\lambda_t = 150$ h^{-1} Mpc, $n = -1.8$.

The mean cluster spectrum reduced to galaxies is presented in Fig. 5. The error analysis presented in detail in the next section shows that the overall rms error of the mean power spectrum at the large-scale end is of the order ± 0.35 in logarithmic scale. On smaller scales the rms error is about ± 0.15. In Fig. 5, we have added a 1.5σ error corridor.

3 ERROR ANALYSIS

3.1 Sampling errors

In determining the power spectrum, sampling errors occur due to decisions to include or exclude a particular object in a

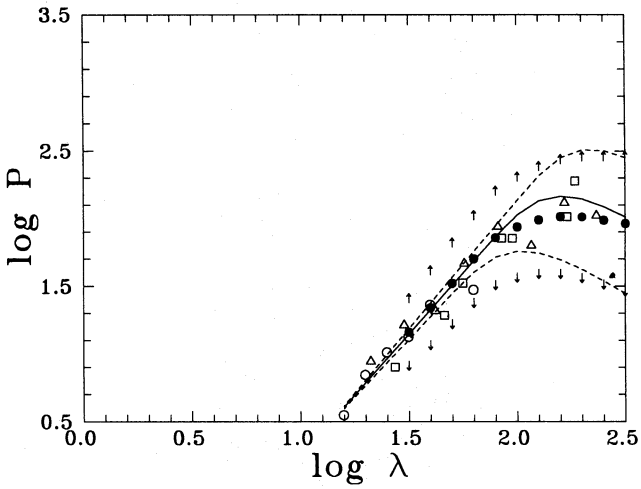

Figure 5. Comparison of the galaxy and cluster spectra reduced to the amplitude of the spectrum for galaxies. Results obtained by BF for galaxies are marked with open circles, radio-galaxy data obtained by PN with triangles, *IRAS* data as reduced by Peacock with squares, cluster spectrum reduced to galaxy spectrum amplitude according to the present paper with filled circles; arrows show the error corridor of the cluster spectrum after reduction to galaxy spectrum amplitude. Solid and dashed lines represent the power law model curves with the transition scales 150 h^{-1} (solid line), 100 h^{-1} (lower dashed line) and 200 h^{-1} Mpc (upper dashed line), respectively.

given volume. A common method for estimating the uncertainty of results due to this effect is the bootstrap procedure. We have calculated the power spectra for 10 subsamples of 200 clusters, each selected at random from the parent samples ACO3N and ACO3S which contain 351 and 427 clusters, respectively. The power spectra were determined from the smoothed density field and corrections for smoothing and Poisson noise were applied. As expected, the sampling error is largest for large-wavelength modes; here the rms sampling error is ± 0.25 in the logarithmic scale, and for smaller wavelengths the rms error is ± 0.10.

3.2 Incompleteness of data

In order to estimate errors due to the incompleteness of data, we shall use weighting of data. The incompleteness is caused by the galactic extinction and by difficulties in finding distant, weak clusters. The galactic extinction decreases the number of Abell clusters, D, selected at low galactic latitudes. This effect can be expressed as

$$D(b) = 10^{\beta(1-1/\sin|b|)}, \tag{9}$$

where b is the galactic latitude and β is a constant (Batuski et al. 1989; West & van den Bergh 1991; Olivier et al. 1990). We have used the value $\beta = 0.32$, and given the clusters in the catalogue a weight inversely proportional to $D(b)$.

A second weight function comes from the spatial density of Abell clusters, which is a function of distance. We have found that up to the distance $r_s = 200\ h^{-1}$ Mpc the spatial density is practically constant (fluctuations can be explained as variations of the real spatial density), but at larger distances the density decreases. The mean density can be expressed in terms of the observed distance interval as follows:

$$D(R) = \begin{cases} 1, & \text{if } r < r_s; \\ 0.5(1 + r_s/r), & \text{if } r \geq r_s. \end{cases} \tag{10}$$

Batuski et al. (1989) find a less marked decrease of the density with distance, but they included only clusters of richness class ≥ 1 in the analysis. We use clusters of all richness classes and therefore the density dependence on distance is stronger. The inverse value of expression (10) has been used as the second weight for clusters.

Weighted spectra for some cluster samples are given in Fig. 6. The correction for distance incompleteness is very small; in other words, the inclusion of clusters of richness class 0 (which are less complete at large distances) introduces only a small systematic error. The better signal-to-noise ratio we obtain is more important. The galactic latitude effect is larger, but again the difference is not too great – at the largest wavelengths, the amplitude can be in error by a factor of ≈ 1.5. Weighting also improves the agreement between samples ACO2N and ACO3N at large wavenumbers.

3.3 Influence of observational errors

The power spectrum is influenced by observational errors of distances estimated from photometric data. To determine the influence of these errors quantitatively, we have artificially distorted distances of clusters in the samples ACO2N and ACO3N, where the number of clusters with estimated redshifts is small. For 20 and 40 per cent of clusters, distance moduli were randomly shifted from their actual values, introducing an error which simulates the influence of errors in photometric distances. The rms shifts in distance modulus were chosen as 0.25 and 0.50 mag. The results of simulations are presented in Fig. 7 for the sample ACO3N. This test shows that observational errors reduce the amplitude of spectra over the whole scale interval, while the reduction rate increases at large wavelengths. The error has a large scatter, i.e. in some runs it was rather small, in other runs larger. In southern samples the fraction of clusters with estimated redshifts is larger than in northern samples, which may partly explain the difference in the spectra. This large error is the main argument in favour of using northern samples.

We can calculate the rms error of the relative amplitude (i.e. the difference in amplitude between the largest scale and

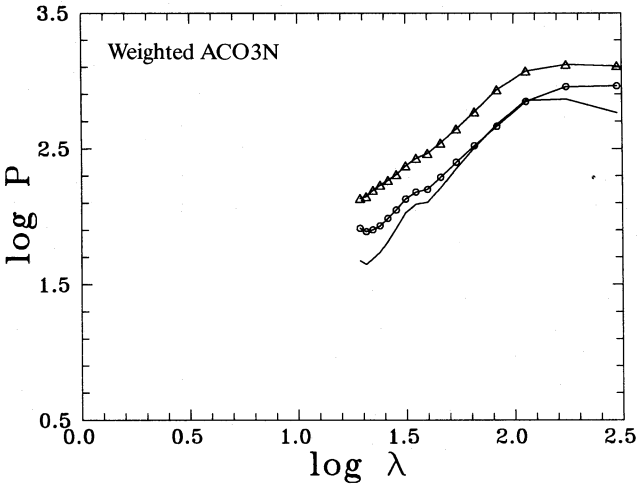

Figure 6. The effect of weighting clusters for sample ACO3N. The solid line shows the unweighted cluster spectrum, and spectra marked with triangles and circles show the effects of using weights for incompleteness near the galactic plane, and distance, respectively.

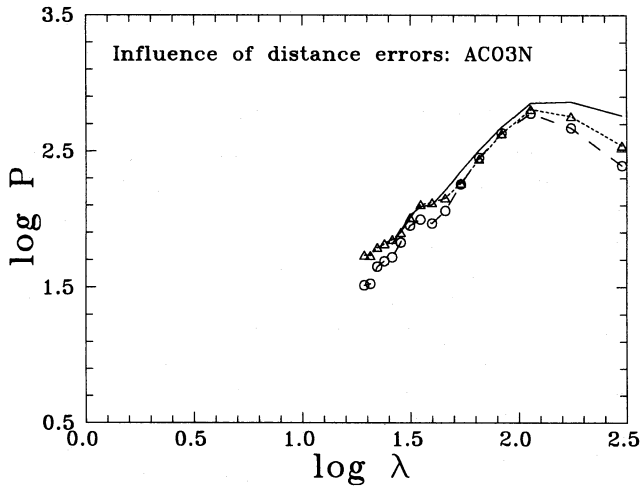

Figure 7. The influence of distance errors for the sample ACO3N: the solid curve gives the observed spectrum, and curves marked with triangles and circles show spectra of subsamples where, for 20 per cent of clusters, distances were randomly distorted supposing distance modulus errors of 0.25 and 0.50 mag, respectively.

some intermediate scale) from the scatter of weighted amplitudes at large wavelengths. The results show that both the scatter due to incompleteness and that due to observational errors are ± 0.15 in logarithmic scale, thus the overall relative error of the amplitude due to these factors is approximately ± 0.25.

There are two ways to reduce this error – to observe more redshifts to avoid clusters with estimated distances, and to increase the sample by including clusters of lower richness, for instance those from the recently completed *ROSAT* X-ray cluster survey.

3.4 The effect of periodic boundary conditions

The algorithm used to calculate the Fourier transform of the density field assumes periodic boundary conditions. This assumption is not valid and may cause systematic errors in the spectrum. To check the possible influence of periodic boundary conditions, Gramann (1992) used high-resolution two-dimensional simulations. She was able to extract, from the total sample, subsamples of various box size in different locations of the sample, and to ask two questions: how large are variations in the power spectra expected to be in different locations, and are there systematic deviations between the spectra of small samples and the spectrum of the total sample? In calculating the spectrum of a subsample, Gramann assumed that the whole Universe consists of replicas of that particular subsample.

The analysis demonstrated that variations in the shape of spectra depend on the linear size of subsamples. If subsamples are smaller than the scale of the maximum of the spectrum, then large variations in the spectrum are observed. On the other hand, if the sample size exceeds the scale of the maximum by a factor of ~ 2, variations between spectra of subsamples are very small, and the mean spectrum of subsamples practically coincides with the spectrum of the parent sample. Visual inspection of respective subsamples shows that there are variations in the structure of small subsamples, but large subsamples have a similar structure. We conclude that periodic boundary conditions exert a minor influence if samples are larger than the transition scale of the spectrum.

3.5 Influence of voids and superclusters

An additional source of errors is the deviation of statistical properties of our samples from mean properties of the Universe, in other words our samples may not be fair samples of the Universe. Analysis by Einasto, Klypin & Saar (1986) and Einasto (1991) has shown that the correlation function of samples of linear size $\approx 60\ h^{-1}$ Mpc depends on their location: in cluster-dominated regions the function lies considerably higher than in void-dominated regions. This suggests that the size of a fair sample must be larger than the size of samples used in this paper. On the other hand, Gramann (1992) has demonstrated that in samples having a linear size which exceeds the transition scale of the power spectrum the power spectrum is fairly constant for different samples; in other words, such samples can be considered as fair samples of the Universe.

Presently, we do not know exactly the size of a fair sample. If our conclusion (see later) that the transition scale of the power spectrum $\lambda_t \approx 150\ h^{-1}$ Mpc is correct, then we must conclude that our $300\ h^{-1}$ Mpc samples can be considered as fair samples. This conclusion is strengthened by the fact that northern and southern diagonal samples have almost identical power spectra. A random error is, however, present; its value, estimated on the basis of the scatter of spectra of diagonal samples, is about ± 0.10.

4 COMPARISON OF CLUSTER POWER SPECTRUM AND CORRELATION FUNCTION WITH MODELS

4.1 Analytical models

Let us compare the observed spectrum of clusters of galaxies with a simple analytical model suggested by GE. For intermediate and large scales, the model can be written as follows:

$$P(k) = A\left(\frac{k}{k_t}\right)^n \{1 - \exp[-(k/k_t)^{1-n}]\}. \qquad (11)$$

P91 used a similar power law for the spectrum which corresponds to the correlation function calculated for the APM survey of galaxies. In our notation, the P91 law has the form

$$P(k) = A\frac{(k/k_t)^n}{1+(k/k_t)^{n-1}}. \qquad (12)$$

Both models are determined by three parameters: (1) the amplitude of the spectrum, A; (2) the scale of the transition, $\lambda_t = 2\pi/k_t$; (3) the power law index, n. On large scales, both formulae reduce to the Harrison–Zeldovich spectrum $P(k) \propto k$. We have used both formulae, and they give rather similar results. To represent the cluster power spectrum, we have varied the transition scale from $\lambda_t = 100\ h^{-1}$ Mpc to $\lambda_t = 200\ h^{-1}$ Mpc. The results are shown in Fig. 5, possible limits of the spectrum being shown by arrows.

4.2 Correlation functions for cluster samples

We have also calculated the correlation functions using the conventional procedure

$$\xi(r) = \frac{N_{cl}(r)}{N_P(r)} - 1, \qquad (13)$$

where $N_{cl}(r)\,dr$ is the number of cluster pairs in a distance interval from r to $r+dr$, and $N_P(r)\,dr$ is the corresponding number in a Poisson sample having identical boundaries with the observed sample.

The correlation lengths of all cluster samples are given in Table 1. A plot of the correlation functions of our basic samples is given in Fig. 8. The error corridor was calculated by the bootstrap method as in Section 3.1, and is given in Fig. 9 for the sample ACO3N.

We have also calculated the power spectra from the observed correlation functions by integrating the correlation function numerically according to formula (6). The resulting spectrum is rather noisy. To improve the numerical accuracy, we have performed another series of calculations by deriving first the power spectrum from the analytic formula (12), and

then the correlation function by integrating formula (5). The resulting correlation functions are plotted in Fig. 9.

4.3 Numerical models

Direct observational data are insufficient to answer the question: how are spectra of clusters of galaxies related to spectra of galaxies and matter? In Section 2, we reduced cluster spectra to those of galaxies and matter. Now we consider this question in more detail using numerical simulations of the evolution of the density field in the Universe.

The methods of performing N-body simulations were described by Gramann (1988, 1992). We used both two- and three-dimensional simulations. The 3D model was calculated in a 64^3 grid with 64^3 particles; in 2D models, a 512^2 grid with 512^2 particles was used, the density parameter being taken as $\Omega = 1$. In 2D models, an index $n = -1$ was used, corresponding in the 3D case to $n = -2$. The spectral index of the 3D model was $n = -1.5$. All models have either a transition to the Harrison–Zeldovich index according to equation (12) at $\lambda_t = L/4$, where L is the size of the computational box, or a sharp cut-off at the same wavelength (model 2D4T).

Our analysis has shown that the resolution of the 3D model was only marginally sufficient for the present analysis, and so we give in Table 2 data for 2D models only. As in our previous papers (Gramann 1988; Einasto et al. 1991), we divide the matter into the clustered and non-clustered components by a certain threshold density, ϱ_t, the respective fraction of matter in the clustered component, F_g, being given in Table 2. A fraction of matter $0.50 \le F_g \le 0.75$ corresponds to galaxies, $F_g \approx 0.15$ to ordinary clusters, $F_g \le 0.05$ to rich clusters of galaxies.

Spectra of subsamples were calculated using the procedure described above. All spectra were reduced to that of the matter by formula (8). For one series of models, results are shown in Fig. 10. We see that, reduced to the matter, the

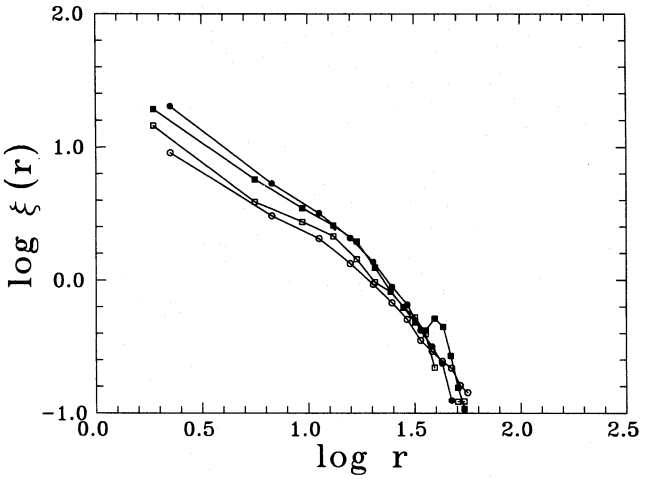

Figure 8. The correlation function of samples ACO2.5N (filled squares), ACO3N (filled circles), ACO2.5S (open squares) and ACO3S (open circles).

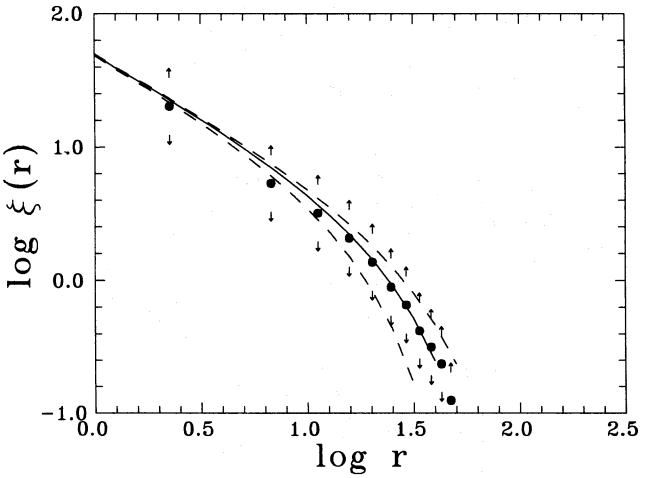

Figure 9. The correlation function of cluster sample ACO3N (filled circles) and its error corridor (arrows). Solid and dashed lines show the correlation functions for the Peacock analytical model, parameters as in Fig. 5, but amplitude is not reduced to the galaxy spectrum.

Table 2. Data on model samples.

Name	λ_t	n	ϱ_t	N	F_g
2D4T.00	$L/4$	-1	0.0	262144	1.0000
2D4T.56	$L/4$	-1	2.0	147725	0.5635
2D4T.14	$L/4$	-1	10.0	37334	0.1424
2D4T.03	$L/4$	-1	20.0	8978	0.0342
2D4.00	$L/4$	-1	0.0	262144	1.0000
2D4.75	$L/4$	-1	1.0	196517	0.7496
2D4.13	$L/4$	-1	10.0	35089	0.1338
2D4.03	$L/4$	-1	20.0	8090	0.0309

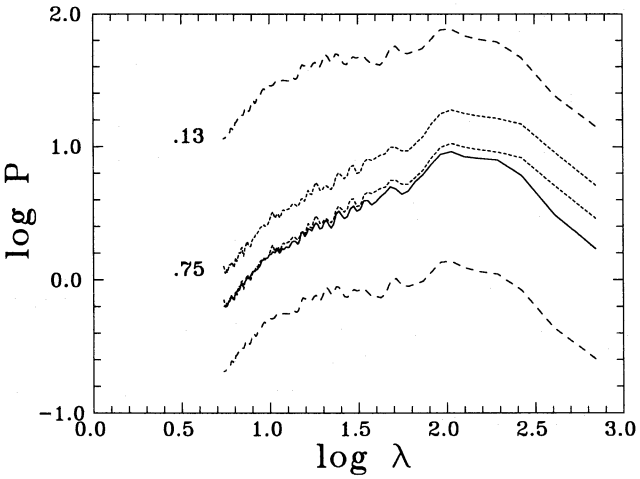

Figure 10. Power spectra for model 2D4 samples. The solid line shows the density spectrum for the total mass, short-dashed lines show the spectra for galaxies, $F_g = 0.75$, and long-dashed lines correspond to the spectra of matter associated with clusters of galaxies, $F_g = 0.13$. Curves above the solid line marked with F_g values correspond to a normalization with respect to the mean density of the sample studied, unmarked curves around and below the solid line to a normalization with respect to the mean density of all matter according to formula (8). Spectra are corrected for smoothing effect and Poisson noise. Note the stability of the maxima of spectra.

galaxy spectrum ($F_g = 0.75$) almost coincides with the spectrum calculated for the whole matter (solid line). In the case of clusters, formula (8) overcorrects the spectrum, and the corrected spectrum lies considerably below the matter spectrum. Thus the reduction rate to the matter spectrum can be derived empirically. The shape of the cluster spectrum is different from the shape of the matter spectrum. Thus, in order to reduce the cluster spectrum to the matter spectrum, two corrections are needed, one for the difference in amplitude, and another for the difference in shape.

In the present paper, we have studied only a relatively short interval of the cluster spectrum (about 10 modes). The differential correction is small (less than 1.5) in this interval, and we ignore it. In this approximation, the cluster spectrum can be reduced to the galaxy spectrum by dividing it by a constant factor. Model calculations are not accurate enough to determine this factor theoretically, and we have used an empirical factor (6.3).

Fig. 10 demonstrates one feature of spectra calculated for populations of different threshold density – the maximum of the spectra is a stable characteristic, and it does not depend on the threshold density level. The same property is observed in all models studied so far. Since the determination of the maximum of the spectrum (transition to the Harrison–Zeldovich spectrum) is one of the main goals of the present study, we can say that the use of clusters as indicators of the spectrum is justified.

5 DISCUSSION

5.1 Transition scale of the cluster power spectrum

The mean observed spectrum agrees well with the model spectrum with $\lambda_t \approx 150\ h^{-1}$ Mpc. Error corridors of the spectrum and the correlation function allow the transition scale to be as low as $100\ h^{-1}$ Mpc and as high as $200\ h^{-1}$ Mpc. Thus we can accept $\lambda_t = 150 \pm 50\ h^{-1}$ Mpc.

The correlation length of the model $\lambda_t = 150\ h^{-1}$ Mpc is $r_0 = 22.6\ h^{-1}$ Mpc. We notice for comparison that West & van den Bergh (1991) obtained for cD galaxy dominated clusters the value $r_0 = 22.1\ h^{-1}$ Mpc, in good agreement with our result. Models with extreme (large or small) transition scales have correlation lengths $r_0 = 18.8\ h^{-1}$ Mpc and $r_0 = 28.3\ h^{-1}$ Mpc, also in good agreement with the error range derived by West & van den Bergh.

Independent evidence for the transition scale comes from the mean distance between deep potential wells and density maxima, which is about 100–150 h^{-1} Mpc (Broadhurst et al. 1990; Bahcall 1991). As demonstrated by Gramann (1992), the mean distance of potential wells is determined by the scale of the maximum of the power spectrum.

5.2 Comparison with power spectra found by previous investigations

The comparison of our results with the results of other recent determinations of the power spectrum is illustrated in Fig. 5, where we plot the galaxy power spectrum found by GE and BF, the power spectrum for radio galaxies found by PN, and the spectrum calculated by P91 for the *IRAS* QDOT redshift survey (Efstathiou et al. 1990); see caption to Fig. 5 for details. We note that PN and P91 used the power spectrum in the form Δ^2; their spectrum was transformed to our notation P and vertically slightly adjusted to bring the spectrum into agreement with the normal galaxy spectrum in the scale interval from ≈ 20 to $\approx 100\ h^{-1}$ Mpc.

Fig. 5 demonstrates excellent agreement between the spectra found for five independent data sets. Practically all estimates of the power spectrum lie within the error corridor calculated for the cluster data.

5.3 The fair-sample problem

According to the definition, a fair sample of the Universe is a sample which has statistically the same properties as the Universe as a whole in our vicinity. Previous studies of the correlation function and the void probability function have shown that these functions differ for samples taken at different locations if the sample size is of the order $\approx 60\ h^{-1}$ Mpc or less (Einasto et al. 1991; Einasto 1991). The power-spectrum analysis of cluster samples presented in this paper demonstrates that northern and southern diagonal samples which are less strongly influenced by incompleteness effects have practically identical power spectra. Thus the empirical evidence indicates that our samples may approach a fair sample of the Universe.

Independent evidence for the size of this sample is given by the power-spectrum analysis itself. If our result concerning the transition scale of the spectrum is correct then we come to the conclusion that the fair sample size is of the order of $\approx 300\ h^{-1}$ Mpc; see Gramann (1992) for numerical analysis of the problem.

6 CONCLUSIONS

The basic results of our analysis can be formulated as follows.

(i) We have applied the power-spectrum analysis to the distribution of Abell clusters. We have developed and/or applied procedures to correct for the smoothing effect, for the Poisson noise, and to estimate the errors due to incompleteness of data and observational errors of distances.

(ii) We have calculated the power spectra and correlation functions for clusters of galaxies in the northern and southern galactic hemispheres. Our results suggest that the spectrum has a transition from the Harrison–Zeldovich spectrum to that of a low index between $100\ h^{-1}$ Mpc and $200\ h^{-1}$ Mpc.

(iii) Direct comparison of the properties of northern and southern cluster samples and power-spectrum analysis suggest that the sizes of our samples may approach the size of fair samples of the Universe.

ACKNOWLEDGMENTS

This work has been partly carried out during visits to the European Southern Observatory and Institute of Astronomy, Cambridge. JE, MG and ET thank Professors Harry van der Laan and Martin Rees for their hospitality. We also thank Drs Ron Olowin and John Huchra for providing their cluster catalogue and redshift survey results prior to publication, and Dr Jaan Pelt for stimulating discussions. Suggestions made by an anonymous referee were useful.

REFERENCES

Abell G., Corwin H., Olowin R., 1989, ApJS, 70, 1
Bahcall N. A., 1991, ApJ, 376, 43
Batuski D. J., Bahcall N. A., Olowin R. P., Burns J. O., 1989, ApJ, 341, 599
Baumgart D. J., Fry J. N., 1991, ApJ, 375, 25
Broadhurst T. J., Ellis R. S., Koo D. C., Szalay A. S., 1990, Nat, 343, 726
Efstathiou G., Kaiser N., Saunders W., Lawrence A., Rowan-Robinson M., Ellis R. S., Frenk C. S., 1990, MNRAS, 247, 10P
Einasto M., 1991, MNRAS, 252, 261
Einasto J., Gramann M., 1991, in Pagel B., ed., NORDITA Workshop on Astrophysics with the NORDIC Optical Telescope, Copenhagen, in press
Einasto J., Jõeveer M., Saar E., 1979, MNRAS, 193, 353
Einasto J., Klypin A. A., Saar E., 1986, MNRAS, 219, 457
Einasto J., Einasto M., Gramann M., Saar E., 1991, MNRAS, 248, 593
Gramann M., 1988, MNRAS, 234, 569
Gramann M., 1992, ApJ, in press
Gramann M., Einasto J., 1991, in Böhringer H., Treumann R. A., eds, Traces of the Primordial Structure in the Universe. MPE Report 227, 7
Gramann M., Einasto J., 1992, MNRAS, 254, 453
Hockney R. W., 1970, in Alder B., Fernbach S., Rotenberg M., eds, Methods in Computational Physics IX; Plasma Physics. Academic Press, New York, p. 135
Leir A. A., van den Bergh S., 1977, ApJS, 34, 381
Olivier S., Blumenthal G. R., Dekel A., Primack J. R., Stanhill D., 1990, ApJ, 356, 1
Peacock J. A., 1991, MNRAS, 253, 1P
Peacock J. A., Nicholson D., 1991, MNRAS, 253, 307
Peebles P. J. E., 1973, ApJ, 185, 413
Peebles P. J. E., 1980, The Large-Scale Structure of the Universe. Princeton Univ. Press, Princeton
Postman M., Huchra J. P., Geller M. J., Henry J. P., 1985, AJ, 90, 1400
Smoot G. F. et al., 1992, ApJ, 396, L1
Tago E., Einasto J., 1992, preprint
Tago E., Einasto J., Saar E., 1984, MNRAS, 206, 559
West M. J., van den Bergh S., 1991, ApJ, 373, 86

APPENDIX: SMOOTHING OF SPECTRA BY THE DENSITY ESTIMATION PROCEDURE

Our initial data consists of the positions of clusters in space. In order to get a smooth density field, we introduced a regular grid with a cell size l and used a well-known CIC procedure to assign masses to grid points. This procedure is, essentially, a convolution of the initial density with the function

$$\omega(x, y, z) = \omega_1(x)\,\omega_1(y)\,\omega_1(z), \tag{A1}$$

where the one-dimensional weighting function $\omega_1(x)$ is given by

$$\omega_1(x) = \begin{cases} l^{-1}(1-|x|/l), & |x|<l; \\ 0, & |x|\geq l. \end{cases} \tag{A2}$$

In the Fourier representation, this convolution leads to multiplication of the true Fourier transform of the density field by the Fourier transform $W(\boldsymbol{k})$ of the function $\omega(x, y, z)$. Once more, this is a product of three one-dimensional Fourier transforms:

$$W(\boldsymbol{k}) = W_1(k_x)\,W_1(k_y)\,W_1(k_z), \tag{A3}$$

where

$$W_1(k) = \frac{2}{k^2 l^2}[1-\cos(kl)]. \tag{A4}$$

As the power spectrum is the integral of the squares of the Fourier amplitudes, the correction for the spectrum will be $W^2(\boldsymbol{k})$. For practical application, we must note that we have assumed that the spectrum we study is isotropic. This is ensured by averaging the real spectrum over all directions. It is easy to see that if we assume that the true density distribution is isotropic (our weighting function is not), then the averaged spectrum

$$P_{\rm est}(k) = \langle P(\boldsymbol{k})\rangle_{S(k)}, \tag{A5}$$

where $S(k)$ is the surface of a sphere of radius k, can be written as

$$P_{\rm est}(k) = P_{\rm true}(k)\langle W^2(\boldsymbol{k})\rangle_{S(k)}. \tag{A6}$$

The latter average $\langle W^2(\boldsymbol{k})\rangle = K(k)$ is the correction we are looking for:

$$K(y) = \frac{2}{\pi y^{12}}\int_0^{\pi/2}\frac{\mathrm{d}\phi}{\cos^4\phi\sin^4\phi}\int_0^{\pi/2}\frac{\mathrm{d}\theta}{\cos^7\theta\sin^4\theta} \times[1-\cos(y\sin\theta)]^2[1-\cos(y\cos\theta\cos\phi)]^2 \times[1-\cos(y\cos\theta\sin\phi)]^2, \tag{A7}$$

where we have used the abbreviation $y = kl$.

We show this correction in Fig. A1 together with a simple approximation $K(k) \approx W_1^2(k)$. This simple expression works well until $y = kl = 2\pi$. After this point, the true correction stays much closer to zero than the one-dimensional approximation would predict.

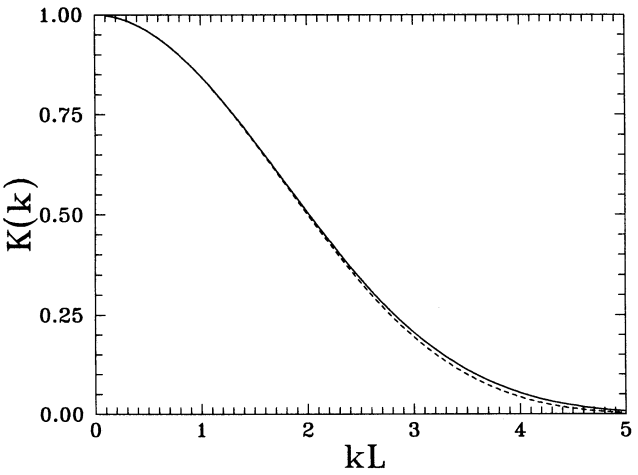

Figure A.1. The correction function for density spectra from the CIC density estimation procedure. The solid line gives the correction for the three-dimensional case, the dashed line a one-dimensional approximation.

The correction factor for grid smoothing can be rather accurately expressed by the following empirical formula:

$$\Delta \log P = 10^{a_0 - b_0 (\log k_{max} - \log k)^c_0}, \qquad \text{(A8)}$$

where $k_{max} = 2\pi/l$ is the maximal wavenumber of the sample for given resolution parameter q. Constant $a_0 = -0.23$ determines the maximal correction at the high-frequency end $k = k_{max}$, and constants $b_0 = 1.95$ and $c_0 = 1.15$ fix the rate of the decrease of the correction for increasing difference in frequency $\log k$. This formula was found by comparison of spectra calculated for different values of the resolution parameter q.